Effect of target localization on the sensitivity of a localized surface plasmon resonance biosensor based on subwavelength metallic nanostructures

Kyung Min Byun,[1] Seong Min Jang,[2] Sung June Kim,[2] and Donghyun Kim[3,*]

[1]*Department of Biomedical Engineering, Kyung Hee University, Yongin, South Korea 446-701*
[2]*Department of Electrical Engineering and Computer Science, Seoul National University, Seoul, South Korea 151-742*
[3]*School of Electrical and Electronic Engineering, Yonsei University, Seoul, South Korea 120-749*
**Corresponding author: kimd@yonsei.ac.kr*

Received November 13, 2008; revised February 17, 2009; accepted February 17, 2009; posted February 20, 2009 (Doc. ID 104043); published March 25, 2009

A localized surface plasmon resonance (LSPR) biosensor using surface relief nanostructures was investigated to evaluate the importance of target localization on the sensitivity enhancement. The LSPR device was modeled as periodic metallic nanowires with a square profile on a gold film and the target as a self-assembled monolayer in buffer solution. The numerical results using rigorous coupled-wave analysis and the finite-difference time domain method demonstrated localized plasmonic fields induced by the surface nanostructure from which the effect of target localization on the sensitivity was quantitatively analyzed. Interestingly, it was found that target localization on nanowire sidewalls improves sensitivity significantly because of strong overlap with localized plasmonic fields. An LSPR structure optimized for a localized target on sidewalls provides sensitivity enhancement per unit target volume by more than 20 times in water ambience. © 2009 Optical Society of America

OCIS codes: 050.2770, 130.6010, 240.6680.

1. INTRODUCTION

Surface plasmons are electromagnetic waves that propagate along the interface between a thin metal film and a dielectric medium. In principle, surface plasmon resonance (SPR) is attributed to the resonant coupling of photons from TM-polarized light to the oscillation of free electrons, which produces a strong evanescent electromagnetic wave on the metal surface [1]. SPR is not excited under TE polarization and appears as a deep minimum in reflectivity tracked by angular or wavelength scanning. Since SPR and its characteristics are very sensitive to the change of dielectric media, this technique can be used to characterize biomolecules immobilized onto a thin metal film. A thin film-based SPR structure has been employed in various sensor applications because of many advantages such as real-time, label-free, and nondestructive detection [2].

Conventional SPR biosensors still have limitations in directly detecting small biochemical interactions at low molecular concentrations. For this reason, various approaches for improving sensitivity have been attempted. For example, nanoparticle-enhanced SPR biosensors incorporating colloidal metallic nanoparticles to excite localized surface plasmons (LSPs) as well as to provide an additional mass during the binding process showed a pronounced SPR angle shift [3,4]. However, the requirement of using nanoparticles on target analytes transforms the advantageous label-free sensing technique into a labeled one. Complex labeling may interfere with biomolecular interactions as the bound nanoparticles affect the binding process directly [5]. Moreover, this method inevitably suffers from irreproducible sensitivity characteristics.

Another approach for enhanced sensitivity is to develop a novel substrate for an SPR biosensor based on the Kretschmann configuration [6]. Newly designed substrates have been introduced to induce a surface-limited increase of reaction area. Oh *et al.* [7] produced a threefold sensitivity improvement by utilizing a mesoporous silica structure on a gold film as a rigid matrix functionalized with a self-assembled monolayer (SAM). While a high pore volume of mesoporous silica substrate can lead to notable amplification in the resonance shift, the results may be difficult to replicate due to randomly distributed silica matrices. Further, its performance is fundamentally based on the excitation of propagating surface plasmons supported by a thin metal film. Thus, significant sensitivity improvement associated with enhanced local fields is essentially infeasible.

In contrast, we have considered surface nanostructures on a metallic film as an alternative substrate by which LSPs are excited. The LSPs interact with propagating surface plasmons on the sensor surface and create hybrid modes. Earlier results suggest that the substrate with periodic nanowires was shown to provide reproducible sensitivity enhancement associated with an increased reaction area and LSP excitation by nanowires [8,9]. In addition, the effects of nanowire period, depth, and volume factor (VF) were investigated in terms of various sensor characteristics, such as sensitivity enhancement factor (SEF), SPR curve angular width (CAW), and

minimum reflectance at resonance (MRR) [10–12]. Note that optimal nanowire structures were determined to yield remarkably improved sensitivity by more than an order in air environments. Its detection property was also found to be quite linear with a refractive index of a target SAM. Recently, Malic *et al.* [13] applied (two-dimensional) 2D gold nanoposts on an SPR imaging biosensor system to demonstrate highly sensitive label-free detection of DNA hybridization.

These studies on a nanostructure-based localized surface plasmon resonance (LSPR) biosensor assumed uniform target distribution [8,10,12,14]. In practice, this assumption may only be valid as long as the target distribution varies slowly. In contrast to the previous approaches, we intend here to address the possibility of localizing targets in the locally enhanced fields so that the target can be more significantly amplified by the surface nanostructure. This is conceptually consistent with the measurement of fluorescent dyes localized in a nanowell [15], although our analysis focuses on the label-free detection of a localized target. Per unit target volume, such target localization is expected to allow sensitivity enhancement that would be difficult to achieve with uniform target distribution. The goal of this paper is thus to numerically explore the enhancement as a result of target localization, whether the localization-induced enhancement is real and the amount of enhancement. For this reason, it is important to investigate the spatial distribution of localized plasmonic fields on a sensor surface and the impact of target presence on the field distribution since the local field amplification by metallic nanostructures is known to contribute to the enhancement of optical transitions in biomolecules within nanoscopic distance from a metallic nanostructure [16]. Potentially, this research can be crucial to taking advantage of localized nanophotonic fields for biomolecular sensing and imaging.

2. NUMERICAL MODEL

The dispersion relation between surface plasmon wavenumber k_{SP} and incident light angular frequency ω can be calculated from Maxwell's equations and is given by

$$k_{SP} = \frac{\omega}{c}\sqrt{\frac{\varepsilon_m \varepsilon_d}{\varepsilon_m + \varepsilon_d}} = k_0 \sin \theta_{SPR}, \quad (1)$$

where θ_{SPR}, ε_m, and ε_d represent the angle of incidence at resonance, metal permittivity, and dielectric permittivity; c and k_0 are for the speed of light and wavenumber in the free space. For an LSPR biosensor with subwavelength metallic nanostructures, ε_d is replaced with ε_{eff} that is a complex number and can be dominantly negative real depending on the VF and the ratio of the volume occupied by gold nanowires per period. While one may use effective medium theories for subwavelength structures, in general, ε_{eff} and thus the dispersion relation of LSPs are not available in a closed form. For this reason, we employed rigorous coupled-wave analysis (RCWA) [17], which has been successfully applied to explain experimental results of nanostructures [18–20]. Our RCWA routine was found to corroborate the experiments of earlier SPR research using gold nanowires [10]. Convergence in RCWA computation was achieved by including 30 space harmonic orders.

The schematic of a nanowire-mediated gold substrate is described in Fig. 1. A one-dimensional (1D) array of infinitely long gold nanowires with a period Λ is assumed to be regularly patterned on a gold film supporting bulk surface plasmons. The thickness of gold and chromium films is fixed at 40 and 2 nm. The chromium layer is adopted to enhance the adhesion between gold and the glass substrate in experiments. TM-polarized light at $\lambda = 633$ nm is incident through an SF10 glass substrate as the incidence angle is scanned with an angular resolution of 0.01° under the total internal reflection condition. Target analytes are modeled as a 1 nm thick SAM. We assumed 1,6-hexanedithiol for the representative dielectric SAM by approximating it as a homogeneous layer with a refractive index $n(\text{SAM}) = 1.52643$ [21]. To investigate the effects of target localization on sensitivity, a SAM is divided into three localization regions: nanowire top, sidewalls, and bottom area between nanowires denoted, respectively, by SAM_T, SAM_S, and SAM_B as presented in Fig. 1(b). SAM_{ALL} represents a uniform target on the surface, i.e., no target localization. The optical constants (n,k) of an

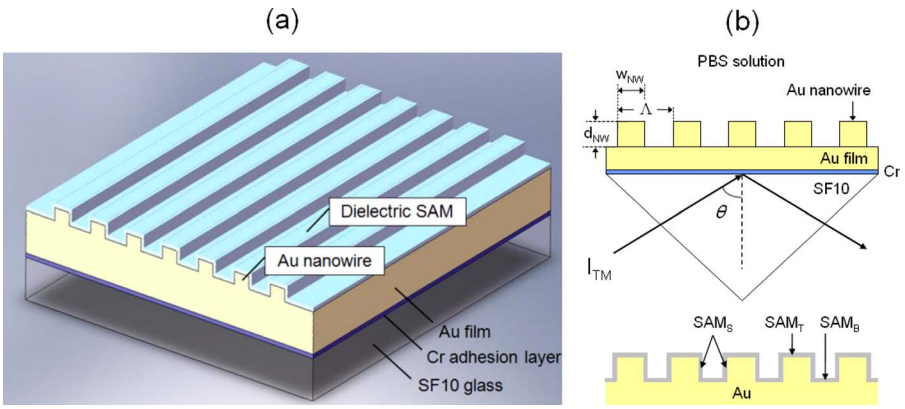

Fig. 1. (Color online) (a) Three-dimensional (3D) schematic of a nanowire-mediated substrate. (b) 2D cross section of the LSPR substrate. TM-polarized light with $\lambda = 633$ nm propagating into an SF10 glass is incident on an attachment layer of chromium (2 nm), a thin gold film (40 nm), 1D gold nanowires, and a 1 nm thick SAM layer covering the whole substrate surface. Gold nanowires of a rectangular profile, assumed to be infinite in length, have a width w_{NW}, a thickness d_{NW}, and a period Λ. A dielectric SAM on top of the nanowire, sidewalls of the nanowire, and on a gold film is denoted by SAM_T, SAM_S, and SAM_B.

SF10 glass substrate, chromium, and gold were taken as (1.7231, 0), (3.48, 4.36), and (0.18, 3.0) at $\lambda = 633$ nm [22]. The refractive index of a phosphate-buffered saline (PBS) solution was assumed to be 1.33. The profile of gold nanowires was simplified as a rectangle of width w_{NW} and depth d_{NW}. Thus, VF is w_{NW}/Λ.

As a quantitative measure of sensitivity improvement, a SEF—the ratio of resonance angle shift due to target binding on a nanowire-based substrate to that of a conventional bare SPR structure assuming a 40 nm thick gold film—is defined as

$$\mathrm{SEF} = \frac{\Delta\theta_{\mathrm{NWSPR}}}{\Delta\theta_{\mathrm{SPR}}} = \frac{\theta_{\mathrm{NWSPR}}(\text{target}) - \theta_{\mathrm{NWSPR}}(\text{no target})}{\theta_{\mathrm{SPR}}(\text{target}) - \theta_{\mathrm{SPR}}(\text{no target})}, \tag{2}$$

where θ_{NWSPR} and θ_{SPR} represent the resonance angle with and without gold nanowires. From the calculated reflectance curves of a conventional SPR configuration, θ_{SPR} (target) $= 59.94°$ and θ_{SPR} (no target) $= 59.75°$; thus $\Delta\theta_{\mathrm{SPR}} = 0.19°$. Molecular quantities of SAM_T, SAM_S, SAM_B, and $\mathrm{SAM}_{\mathrm{ALL}}$ are all different per the unit period of nanograting, and the amount depends on various geometrical parameters, such as grating thickness and period. While SEF represents the enhancement that is measured macroscopically when light is incident on an identical surface area for LSPR and conventional SPR structures, true enhancement of sensitivity is the sensitivity per unit target volume, i.e., the SEF scaled with the quantities involved in the biomolecular interaction of interest. Therefore, we define the sensitivity enhancement per unit target volume ($\mathrm{SEF}_{\mathrm{UTV}}$) as

$$\mathrm{SEF}_{\mathrm{UTV}} = \frac{\Delta\theta_{\mathrm{NWSPR}}/V_{\mathrm{NWSPR}}}{\Delta\theta_{\mathrm{SPR}}/V_{\mathrm{SPR}}}, \tag{3}$$

where V_{NWSPR} and V_{SPR} denote the total target volume for LSPR and conventional SPR structures. Although a SAM is assumed to cover an infinite sensor surface, the ratio of the total surface reaction area of an LSPR structure to that of a SPR structure (i.e., $V_{\mathrm{NWSPR}}/V_{\mathrm{SPR}}$) remains constant regardless of the surface dimension. Thus, the reaction volume per period can be substituted for the total target volume in Eq. (3). For the periodic nanowires shown in Fig. 1, $\mathrm{SEF}_{\mathrm{UTV}}$ ($\mathrm{SAM}_{\mathrm{ALL}}$) can be simplified as

$$\mathrm{SEF}_{\mathrm{UTV}}(\mathrm{SAM}_{\mathrm{ALL}}) = \frac{\Delta\theta_{\mathrm{NWSPR}}/(\Lambda + 2d_{\mathrm{NW}})}{\Delta\theta_{\mathrm{SPR}}/\Lambda} = \frac{\mathrm{SEF}(\mathrm{SAM}_{\mathrm{ALL}}) \cdot \Lambda}{\Lambda + 2d_{\mathrm{NW}}}. \tag{4}$$

For SAM_T, SAM_S, and SAM_B, $\mathrm{SEF}_{\mathrm{UTV}}$ is given by

$$\mathrm{SEF}_{\mathrm{UTV}}(\mathrm{SAM}_T) = \frac{\Delta\theta_{\mathrm{NWSPR}}/(\Lambda \cdot \mathrm{VF})}{\Delta\theta_{\mathrm{SPR}}/\Lambda} = \frac{\mathrm{SEF}(\mathrm{SAM}_T)}{\mathrm{VF}}, \tag{5}$$

$$\mathrm{SEF}_{\mathrm{UTV}}(\mathrm{SAM}_S) = \frac{\Delta\theta_{\mathrm{NWSPR}}/2d_{\mathrm{NW}}}{\Delta\theta_{\mathrm{SPR}}/\Lambda} = \frac{\mathrm{SEF}(\mathrm{SAM}_S) \cdot \Lambda}{2d_{\mathrm{NW}}}, \tag{6}$$

$$\mathrm{SEF}_{\mathrm{UTV}}(\mathrm{SAM}_B) = \frac{\Delta\theta_{\mathrm{NWSPR}}/\Lambda(1 - \mathrm{VF})}{\Delta\theta_{\mathrm{SPR}}/\Lambda} = \frac{\mathrm{SEF}(\mathrm{SAM}_B)}{1 - \mathrm{VF}}. \tag{7}$$

In short, $\mathrm{SEF}_{\mathrm{UTV}}$ is the sensitivity enhancement normalized by the target volume and represents enhanced sensitivity induced by the unit volume of target analytes. To the first degree, $\mathrm{SEF}_{\mathrm{UTV}}$ excludes the effect of reaction area on the sensitivity and directly addresses the contribution of localized plasmons to sensitivity improvement. Both SEF and $\mathrm{SEF}_{\mathrm{UTV}}$ are important for practicality. Note that $\mathrm{SEF}_{\mathrm{UTV}}$ for SAM_S depends on its period and thickness while $\mathrm{SEF}_{\mathrm{UTV}}$ for SAM_T and SAM_B is affected by a VF.

3. RESULTS

A. Effect of Nanowire Thickness

Figure 2 shows SPR reflectance curves of a conventional SPR and a nanowire-based LSPR structure when nanowires have a period of $\Lambda = 50$ nm and VF $= 0.5$. VF $= 0.5$ was selected as a representative value for the nanowire structure because of relative ease in terms of implementation. If target analytes form a uniform film coverage on the whole sensor surface (i.e., $\mathrm{SAM}_{\mathrm{ALL}}$), θ_{NWSPR} (target) $= 64.49°$ and θ_{NWSPR} (no target) $= 63.37°$ at $d_{\mathrm{NW}} = 5$ nm, i.e., SEF $= 5.895$ and $\mathrm{SEF}_{\mathrm{UTV}} = 4.913$. At $d_{\mathrm{NW}} = 10$ nm, θ_{NWSPR} (target) $= 77.00°$ and θ_{NWSPR} (no target) $= 75.39°$; thus SEF $= 8.474$ and $\mathrm{SEF}_{\mathrm{UTV}} = 6.053$. Note that SPR characteristics, such as MRR, SPR, and CAW, are significantly affected by the presence of nanowires. Even though a higher SEF may be obtained with nanowires for $d_{\mathrm{NW}} > 10$ nm, the SPR characteristics of these structures are suboptimal for practical applications due to a large MRR and extremely broad CAW.

To analyze the effect of target localization, SEF and $\mathrm{SEF}_{\mathrm{UTV}}$ were calculated from SPR reflectance curves for each region of target localization as listed in Table 1. $\mathrm{SEF}(\mathrm{SAM}_{\mathrm{ALL}})$ increases with nanowire thickness because

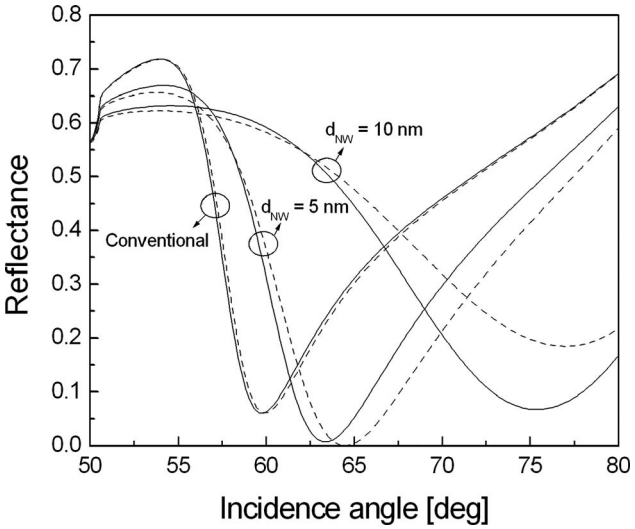

Fig. 2. SPR reflectance curves of a conventional and nanowire-mediated substrate. Nanowires have a period of $\Lambda = 50$ nm and VF $= 0.5$. The solid and dashed curves represent without and with a target, respectively.

Table 1. SEF and SEF_{UTV} Values Calculated for Target Attachment of SAM_T, SAM_B, SAM_S, and SAM_{ALL} When $\Lambda=50$ nm and VF=0.5

	SAM_T		SAM_B		SAM_S		SAM_{ALL}	
d_{NW} [nm]	SEF	SEF_{UTV}	SEF	SEF_{UTV}	SEF	SEF_{UTV}	SEF	SEF_{UTV}
5	1.421	2.842	1.579	3.158	2.684	13.420	5.895	4.913
10	2.947	5.894	2.895	5.790	5.684	14.210	8.474	6.053

of an increment of overall reaction area. SEF(SAM_S) is of particular interest since the effect of SAM_S on the sensitivity has not been evaluated previously. It is intriguing to find that more than 50% of the sensitivity enhancement is associated with the target localized on sidewalls. SEF_{UTV}(SAM_S) is by far the highest among those presented in Table 1. A target SAM present on nanowire sidewalls enhances the sensitivity by more than an order, compared to a conventional SPR biosensor, on a unit volume basis. We believe that this is an indication of enhanced surface fields induced by LSPs that overlap localized target.

To confirm this, we visualize enhanced electromagnetic fields near the sensor surface by calculating the spatial distributions of E_X, H_Y, and E_Z based on the finite-difference time domain (FDTD) method. The minimum grid size for the FDTD was 0.5 nm. Figure 3 shows the field distribution of E_Z at $\theta_{NWSPR}=63.37°$ for nanowires with VF=0.5, $\Lambda=50$ nm, and $d_{NW}=5$ nm and presents well-known features of LSPs excited at a metallic nanostructure that are quite typical of the fields of nonregular structures [23]. On the assumption of an incident electric field of unit amplitude, maximum field amplitudes obtained by FDTD were $E_X=72$, $H_Y=11$, and $E_Z=50$.

What is as important as field enhancement in the context of this paper is where these maxima occur. Obviously, the amplitude of plasmon waves decays rapidly when one moves further away from the nanostructure surface. Since locally enhanced plasmons called "hot spots" [24,25] are distributed at very short distances from the surface, only a limited number of biomolecules within the local fields participate in the resonance shift of an LSPR biosensor, even if a large number of molecules are involved in the interaction. The results shown in Fig. 3 indicate that all maxima are located within 1 nm from the surface in the vicinity of vertices. Because of the field enhancement on nanowire sidewalls, biomolecules on sidewalls participate more vigorously on average than those on nanowire tops and bottoms. As a result, an efficient interplay between target analytes and enhanced LSPs leads to the most prominent improvement of sensitivity with target localization. This poses an interesting postulate that even if there are more biomolecules or thicker SAMs, the resonant shift may not increase proportionately. The strongest enhancement for SAM_S can also be interpreted in terms of the number of resonance peaks, i.e., SAM_S can interact with four LSP modes near the vertices of a nanowire while SAM_T or SAM_B faces two LSP modes at the upper or the lower corners of a nanowire. Note that there are in fact multiple peaks associated with each corner in Fig. 3. Since the decay length of an LSP resonance from the surface of a metallic nanostructure is longer than the interpeak distance, the multiple peaks of each corner as a whole should be regarded as an individual LSP resonance.

Similar to the case of $\Lambda=50$ nm, nanowires at $\Lambda=100$ nm show an increasing SEF with d_{NW} and the maximum SEF_{UTV} for SAM_S as listed in Table 2. In most cases, SEF and SEF_{UTV} at $\Lambda=100$ nm are smaller than those of $\Lambda=50$ nm. Higher SEF and SEF_{UTV} at $\Lambda=50$ nm are mainly attributed to more efficient LSP excitations. For $d_{NW}=10$ nm, field enhancement at $\Lambda=100$ nm is found to be greater than that at $\Lambda=50$ nm, leading to a larger SEF_{UTV} for SAM_S and SAM_{ALL}.

Summarizing this subsection, nanowires with a larger thickness tend to produce more efficient LSP modes, which is consistent with the findings in [12]. The enhancement may be degraded for a larger nanowire period.

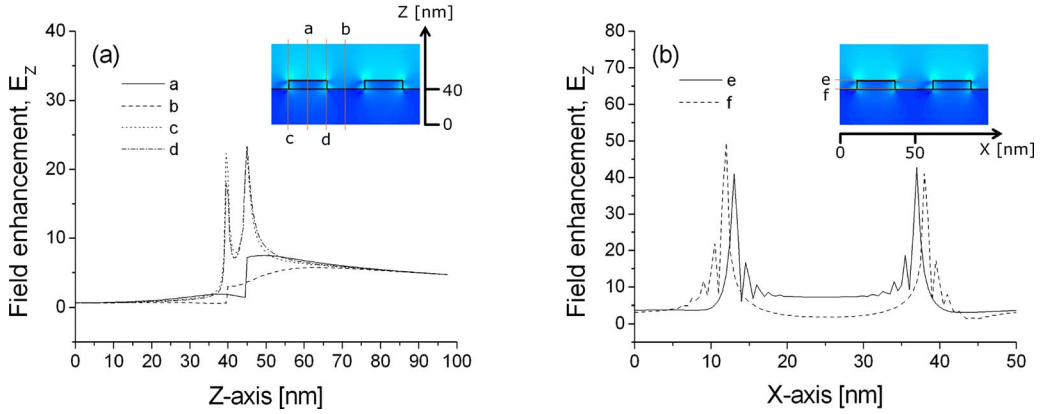

Fig. 3. (Color online) (a) Vertical and (b) horizontal field intensity distribution of E_Z around the sensor surface for nanowires with $\Lambda=50$ nm, VF=0.5, and $d_{NW}=5$ nm. The insets are 2D images obtained from FDTD calculations normalized by the field intensity of 20.

Table 2. SEF and SEF_{UTV} Values Calculated for Target Attachment of SAM_T, SAM_B, SAM_S, and SAM_{ALL} When $\Lambda = 100$ nm and VF = 0.5

d_{NW} [nm]	SAM_T		SAM_B		SAM_S		SAM_{ALL}	
	SEF	SEF_{UTV}	SEF	SEF_{UTV}	SEF	SEF_{UTV}	SEF	SEF_{UTV}
5	1.000	2.000	0.947	1.894	1.158	11.580	3.211	2.919
10	2.316	4.632	2.474	4.948	4.263	21.315	9.474	7.895

B. Effect of Volume Factor

Now we turn our attention to the effect of VFs. Previously, it was reported that the sensitivity improvement of a nanowire-based LSPR biosensor is affected by two major mechanisms of resonant excitations of LSP modes, (1) interaction of propagating surface plasmons in a metal film and LSP modes in nanowires and (2) LSP–LSP coupling between neighboring nanowires [26]. Since these interactions were found to be significant at VF = 0.1 and 0.9 [23,27], we focus on nanowire structures at the two VFs.

Figure 4(a) plots SEF characteristics for VF = 0.1 at $\Lambda = 50$ nm. First of all, destructive coupling between nanowires and target analytes occurs at $d_{NW} = 5$ nm. An opposite shift of resonances was incurred, which is possibly associated with LSP modes driven out of phase [28]. Such a negative shift of resonance was noted as back bending and observed experimentally in a LSPR biosensor using nanoparticles as well [3,4,29].

For $d_{NW} > 5$ nm, Fig. 4(a) shows that $SEF(SAM_T)$ is very poor because the interaction is surface-limited. For SAM_B, enhanced sensitivity was achieved by larger than five times that of a conventional SPR biosensor. $SEF(SAM_S)$ is comparable with $SEF(SAM_B)$ and shows a gentle slope with nanowire thickness due to an increasing reaction area. For SAM_{ALL}, SEF gradually increases up to 12.842 until d_{NW} reaches 30 nm. $SEF(SAM_{ALL})$ saturates for $d_{NW} > 30$ nm as localized electromagnetic fields experience intensity amplification limited by absorption properties for thick gold nanowires. At VF = 0.1, excited plasmons are well isolated around a single nanowire. The local fields interacting with a SAM may lead to a larger change in resonance angles and consequently show prominent sensitivity improvement by more than ten times. It should be emphasized that SEF larger than an order in water environments is accomplished by simply involving target analytes localized at the nanowire sidewalls.

Figure 4(b) shows SEF_{UTV} for a localized SAM. $SEF_{UTV}(SAM_S)$ has an optimum of 10.133 at $d_{NW} = 10$ nm. For $d_{NW} > 10$ nm, $SEF_{UTV}(SAM_S)$ is decreased with an increasing nanowire thickness as dictated by Eq. (6). While sensitivity enhancement per unit volume induced by excited LSP modes occurs most efficiently at the sidewalls until d_{NW} reaches 20 nm, $SEF_{UTV}(SAM_S)$ becomes less important for thicker nanowires. Additionally, it is interesting to see that $SEF_{UTV}(SEF_{ALL})$ is not significantly reduced by d_{NW}, although it is affected by d_{NW} in Eq. (4). This is because the nanowire period in the denominator of Eq. (4) is more dominant for shallow nanowires than the thickness. On the other hand, when $d_{NW} > 25$ nm, both $SEF_{UTV}(SAM_S)$ and $SEF_{UTV}(SAM_{ALL})$ show similar trends as they are highly influenced by the nanowire thickness. While not shown here, SEF_{UTV} as well as SEF are degraded when $d_{NW} > 40$ nm due to the absorption of gold nanowires.

Figure 5 illustrates the FDTD results when VF = 0.1 and $d_{NW} = 30$ nm. The intensity of enhanced fields at the lower vertices of a nanowire is notably larger than at the upper nanowire corners so that SEF_{UTV} for target layers overlapping the two main resonances, i.e., $SEF_{UTV}(SAM_B)$ and $SEF_{UTV}(SAM_S)$ can play an important role in achieving an improvement of the overall sensor sensitivity. This is consistent with the results in Fig. 4.

In contrast, Fig. 6 shows SEF and SEF_{UTV} of VF = 0.9 at $\Lambda = 50$ nm. Although SEFs are smaller than those at VF = 0.1, the highest $SEF(SAM_{ALL}) = 7.789$ was obtained at

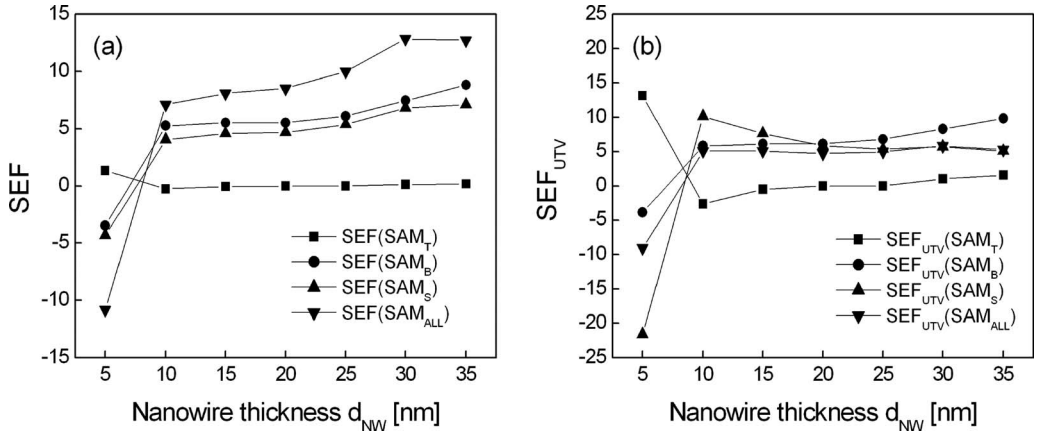

Fig. 4. Characteristics of (a) SEF and (b) SEF_{UTV} with respect to target localization when a nanowire thickness varies at $\Lambda = 50$ nm and VF = 0.1.

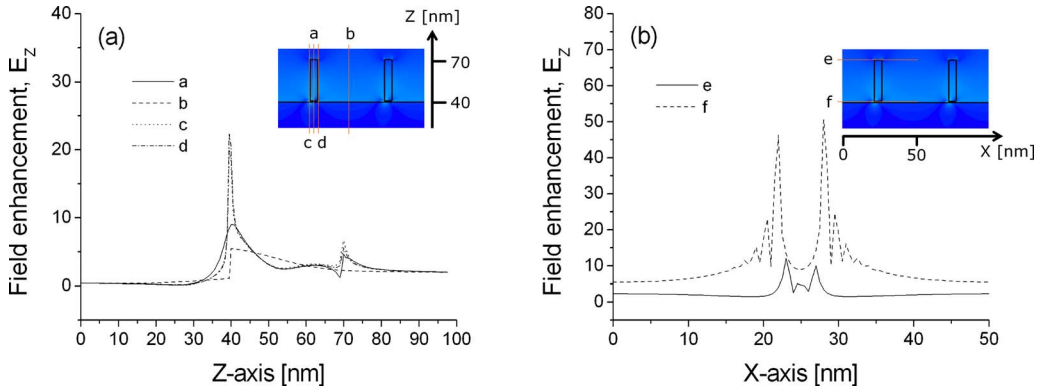

Fig. 5. (Color online) (a) Vertical and (b) horizontal field intensity distribution of E_Z around the sensor surface for nanowires with $\Lambda = 50$ nm, VF = 0.1, and $d_{NW} = 30$ nm. The insets are 2D images obtained from FDTD calculations normalized by the field intensity of 20.

$d_{NW} = 35$ nm. However, since a nanowire-based LSPR biosensor with $d_{NW} > 20$ nm exhibits shallow MRR and extremely broad CAW, feasible maximum SEF in practical applications may be rather 4.737 at $d_{NW} = 15$ nm. SEF(SAM_S) shows a minor increase with nanowire thickness due to an increasing surface reaction area. A low SEF for the SAM_B was also found at VF = 0.9 on account of a narrow interaction area. In Fig. 6(b), SAM_S presents enhanced SEF_{UTV} at small d_{NW} and a maximum of 3.597 at $d_{NW} = 15$ nm. For $d_{NW} > 15$ nm, however, $SEF_{UTV}(SAM_S)$ is decreased with a larger nanowire thickness by Eq. (6). A very low $SEF_{UTV}(SAM_S)$ at $d_{NW} = 10$ nm is derived from zero sensitivity associated with a negative SEF. Also, the variation of $SEF_{UTV}(SAM_{ALL})$ with d_{NW} is limited at VF = 0.9 because the influence of d_{NW} on SEF_{UTV} is less significant when d_{NW} is small as shown in Eq. (4). Moreover, monotonically increasing $SEF(SAM_{ALL})$ for thicker nanowires causes a disparity between $SEF_{UTV}(SAM_S)$ and $SEF_{UTV}(SAM_{ALL})$ compared with the results in Fig. 4(b).

Figure 7 displays stronger localized fields at the upper corners of a nanowire with VF = 0.9 and $d_{NW} = 15$ nm. Depending on the position of the LSP modes, $SEF_{UTV}(SAM_B)$

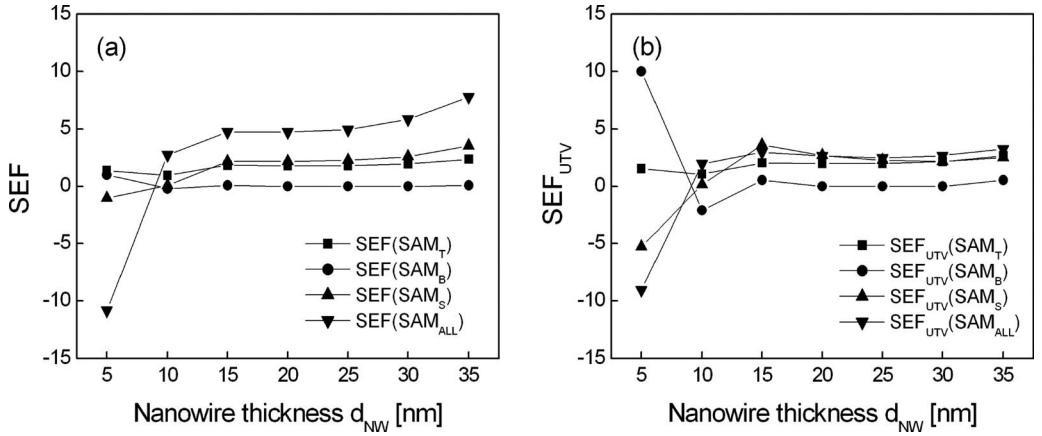

Fig. 6. Characteristics of (a) SEF and (b) SEF_{UTV} with respect to target localization when a nanowire thickness varies at $\Lambda = 50$ nm and VF = 0.9.

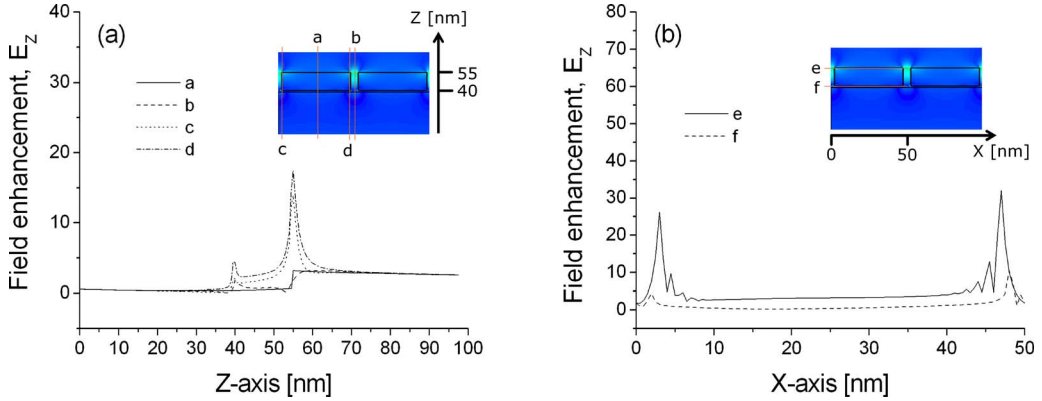

Fig. 7. (Color online) (a) Vertical and (b) horizontal field intensity distribution of E_Z around the sensor surface for nanowires with $\Lambda = 50$ nm, VF = 0.9, and $d_{NW} = 15$ nm. The insets are 2D images obtained from FDTD calculations normalized by the field intensity of 20.

is the smallest, which is consistent with Fig. 6. On the other hand, $SEF_{UTV}(SAM_T)$ is large because a SAM_T on the nanowire top interacts with resonantly enhanced plasmon fields. Also, constructive interactions between highly excited LSP modes and target on sidewalls lead to significant $SEF_{UTV}(SAM_S)$. Note that the maximum field enhancement appears at the upper corners of nanowires in Fig. 7 while it is at the lower corners in Fig. 5. This is because localized plasmons excited in neighboring ridges are coupled at VF=0.9. On the other hand, at VF=0.1, it is rather the interaction of the LSP with propagating surface plasmons that is dominant.

In summary, for both cases of VF=0.1 and 0.9, a target SAM on nanowire sidewalls makes a significant contribution to the overall sensitivity enhancement. A higher SEF is obtained with VF=0.1. For $\Lambda=100$ nm, overall trends, though the results are not shown here, are consistent with those of $\Lambda=50$ nm.

4. DISCUSSION

In terms of actual application, it may be desired to explore small-signal sensitivity, defined as the ratio of resonance angle shift, to small refractive index changes of n(SAM) in PBS environments. Since SPR characteristics depend on LSPs and are accompanied with nonlinear effects, such as resonance broadening and shallow reflectance at resonance, a nanowire-based LSPR biosensor may also suffer from nonlinear sensitivity [13]. In principle, a resonance angle is nonlinear with n(SAM) as stipulated by the dispersion relation of surface plasmons [1].

Considering that SAM_S plays a critical role in achieving a significant improvement of SEF and SEF_{UTV} and also that the difficulties in fabrication are reduced at a longer nanowire period and a VF$\sim$0.5, optimized nanowires for target localization of SAM_S would be $\Lambda=100$ nm, VF=0.5, and $d_{NW}=10$ nm. From Table 2, this structure presents $SEF(SAM_S)=4.263$ and $SEF_{UTV}(SAM_S)=21.315$. This $SEF(SAM_S)$ is relatively high while the $SEF_{UTV}(SAM_S)$ is the largest among those obtained here.

Figure 8(a) shows an SPR angle shift $\delta\theta$ of a conventional SPR and a nanowire-based LSPR structure with such optimal nanowires. For a localized target of SAM_S, a nanowire-mediated LSPR biosensor presents a stiffer slope indicating higher sensitivity for a wide range of binding events on the nanowire sidewalls compared to a conventional one with a uniform SAM coverage. On the other hand, since many biomolecular interactions generally result in a very small change of refractive index, small-signal sensitivity at the narrow range of n(SAM) may be more important [13]. To consider this, the refractive index of a 1 nm thick SAM has been assumed to change from 1.33 to 1.70 in PBS solution, a sufficiently wide range for biomolecular SAMs that come in different lengths and end groups, for instance, as shown in [30]. Figure 8(b) shows small-signal sensitivity $\delta\theta/\delta n$(SAM). While a conventional SPR structure suffers from low small-signal sensitivity with n(SAM), that of a nanowire-mediated substrate rises up to 4.8 and saturates when $n(\text{SAM})>1.6$. As a result, small-signal sensitivity enhancement factor SEF_{small}, defined as $(\delta\theta/\delta n)_{LSPR}/(\delta\theta/\delta n)_{SPR}$, is between 3.895 and 7.848 as shown in Fig. 8(b). From linear regression analyses, it was found that $\delta\theta$ is extremely linear with n(SAM), as R is larger than 0.99, where R is the correlation coefficient that denotes the linearity obtainable in the sensor performance.

Experimentally, target localization can be realized by use of soft lithography techniques, such as microcontact printing, nanotransfer printing, and proximity field nanopatterning [31]. For example, targets on the nanowire top and bottom can be formed by direct printing or masking techniques and targeting on the nanowire sidewalls by applying selective etch processes to uniformly distributed target molecules on the sensor surfaces.

5. CONCLUSION

In this paper, we investigated the effect of target localization on the sensitivity characteristics of a nanowire-mediated LSPR substrate. The target on the nanowire sidewalls, represented by SAM_S, makes a significant contribution to overall sensitivity enhancement. In terms of the sensitivity per unit target volume, target localization on sidewalls takes advantage of plasmonic field localization, which can lead to extremely high enhancement of

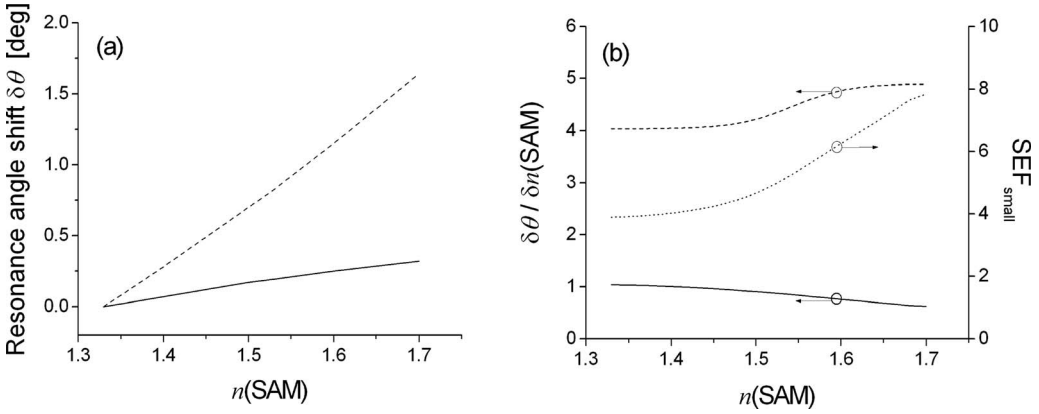

Fig. 8. (a) Resonance angle shift and (b) small-signal sensitivity of a conventional (solid curve) and a nanowire-mediated SPR biosensor (dashed curve) and SEF_{small} (dotted curve) when a refractive index of target analytes bound to the nanowire sidewalls varies from 1.33 to 1.70. Nanowires have a period of $\Lambda=100$ nm, VF=0.5, and $d_{NW}=10$ nm.

sensitivity. For example, a nanowire structure optimized for target localization of SAM_S with $\Lambda = 100$ nm, VF = 0.5, and $d_{NW} = 10$ nm was found to produce a large $SEF(SAM_S)$ of 4.263 and the highest $SEF_{UTV}(SAM_S) = 21.315$. This paper clearly demonstrates a potential for implementing a highly sensitive SPR biosensor with surface relief nanowires by localizing target biomolecules.

ACKNOWLEDGMENTS

This work was supported by the Korea Research Foundation grant funded by the Korean Government Basic Research Promotion Fund (MOEHRD)-(KRF-2008-331-D00229). D. Kim acknowledges support by the Korea Science and Engineering Foundation (KOSEF) through the National Core Research Center for Nanomedical Technology (R15-2004-024-00000-0), KOSEF 2007-8-1158, and R01-2007-000-20821-0 funded by the Korean Government Ministry of Science and Technology (MOST). Partial support was provided by the "System IC 2010" project of Ministry of Knowledge Economy and by the MEMS Research Center for National Defense funded by the Defense Acquisition Program Administration under 2006-MM-41-5ND0600407. S. M. Jang and S. J. Kim were supported by the KOSEF through the Nano Bioelectronics and Systems Research Center (NBS-ERC) at Seoul National University.

REFERENCES

1. H. Raether, *Surface Plasmon on Smooth and Rough Surfaces and on Gratings* (Springer-Verlag, 1988), chap. 2.
2. S. Ekgasit, C. Thammacharoen, F. Yu, and W. Knoll, "Evanescent field in surface plasmon resonance and surface plasmon field-enhanced fluorescence spectroscopies," Anal. Chem. **76**, 2210–2219 (2004).
3. L. A. Lyon, D. J. Pena, and M. J. Natan, "Surface plasmon resonance of Au colloid-modified Au films: particle size dependence," J. Phys. Chem. B **103**, 5826–5831 (1999).
4. L. He, M. D. Musick, S. R. Nicewarner, F. G. Salinas, S. J. Benkovic, M. J. Natan, and C. D. Keating, "Colloidal Au-enhanced surface plasmon resonance for ultrasensitive detection of DNA hybridization," J. Am. Chem. Soc. **122**, 9071–9077 (2000).
5. X. D. Hoa, A. G. Kirk, and M. Tabrizian, "Towards integrated and sensitive surface plasmon resonance biosensors: a review of recent progress," Biosens. Bioelectron. **23**, 151–160 (2007).
6. E. Kretschmann and H. Raether, "Radiative decay of non-radiative surface plasmons excited by light," Z. Naturforsch. A **23A**, 2135–2136 (1968).
7. S. Oh, J. Moon, T. Kang, S. Hong, and J. Yi, "Enhancement of surface plasmon resonance (SPR) signals using organic functionalized mesoporous silica on a gold film," Sens. Actuators B **114**, 1096–1099 (2006).
8. K. M. Byun, S. J. Kim, and D. Kim, "Design study of highly sensitive nanowire-enhanced surface plasmon resonance biosensors using rigorous coupled wave analysis," Opt. Express **13**, 3737–3742 (2005).
9. K. M. Byun, S. J. Yoon, D. Kim, and S. J. Kim, "Experimental study of sensitivity enhancement in surface plasmon resonance biosensors by use of periodic metallic nanowires," Opt. Lett. **32**, 1902–1904 (2007).
10. K. M. Byun, S. J. Kim, and D. Kim, "Profile effect on the feasibility of extinction based localized surface plasmon resonance biosensors using metallic nanowires," Appl. Opt. **45**, 3382–3389 (2006).
11. K. M. Byun, D. Kim, and S. J. Kim, "Investigation of the profile effect on the sensitivity enhancement of nanowire-mediated localized surface plasmon resonance biosensors," Sens. Actuators B **117**, 401–407 (2006).
12. K. Kim, S. J. Yoon, and D. Kim, "Nanowire-based enhancement of localized surface plasmon resonance for highly sensitive detection: a theoretical study," Opt. Express **14**, 12419–12431 (2006).
13. L. Malic, B. Cui, T. Veres, and M. Tabrizian, "Enhanced surface plasmon resonance imaging detection of DNA hybridization on periodic gold nanoposts," Opt. Lett. **32**, 3092–3094 (2007).
14. S. J. Yoon and D. Kim, "Target dependence of the sensitivity in periodic nanowire-based localized surface plasmon resonance biosensors," J. Opt. Soc. Am. A **25**, 725–735 (2008).
15. M. J. Levene, J. Korlach, S. W. Turner, M. Foquet, H. G. Craighead, and W. W. Webb, "Zero-mode waveguides for single-molecule analysis at high concentrations," Science **299**, 682–686 (2003).
16. P. N. Prasad, *Nanophotonics* (Wiley-Interscience, 2004), Chap. 5.
17. M. G. Moharam and T. K. Gaylord, "Rigorous coupled-wave analysis of metallic surface-relief gratings," J. Opt. Soc. Am. A **3**, 1780–1787 (1986).
18. P. J. Valle, F. Moreno, J. M. Saiz, and F. González, "Near-field scattering from subwavelength metallic protuberances on conducting flat substrates," Phys. Rev. B **51**, 13681–13690 (1995).
19. Y. Kanamori, K. Hane, H. Sai, and H. Yugami, "100 nm period silicon antireflection structures fabricated using a porous alumina membrane mask," Appl. Phys. (N.Y.) **78**, 142–143 (2001).
20. J. Cesario, R. Quidant, G. Badenes, and S. Enoch, "Electromagnetic coupling between a metal nanoparticles grating and a metallic surface," Opt. Lett. **30**, 3404–3406 (2005).
21. E. Hutter, S. Cha, J.-F. Liu, J. Park, J. Yi, J. H. Fendler, and D. Roy, "Role of substrate metal in gold nanoparticle enhanced surface plasmon resonance imaging," J. Phys. Chem. B **105**, 8–12 (2001).
22. E. D. Palik, *Handbook of Optical Constants of Solids* (Academic, 1985).
23. J. P. Kottmann, O. J. F. Martin, D. R. Smith, and S. Schultz, "Plasmon resonances of silver nanowires with a nonregular cross section," Phys. Rev. B **64**, 235402 (2001).
24. L. Qin, S. Zou, C. Xue, A. Atkinson, G. C. Schatz, and C. A. Mirkin, "Designing, fabricating, and imaging Raman hot spots," Proc. Natl. Acad. Sci. U.S.A. **103**, 13300–13303 (2006).
25. E. Hao and G. C. Schatz, "Electromagnetic fields around silver nanoparticles and dimers," J. Chem. Phys. **120**, 357–366 (2004).
26. D. Kim, "Effect of resonant localized plasmon coupling on the sensitivity enhancement of nanowire-based surface plasmon resonance biosensors," J. Opt. Soc. Am. A **23**, 2307–2314 (2007).
27. K. M. Byun, M. L. Shuler, S. J. Kim, S. J. Yoon, and D. Kim, "Sensitivity enhancement of surface plasmon resonance imaging using periodic metallic nanowires," J. Lightwave Technol. **26**, 1472–1478 (2008).
28. J. P. Kottmann and O. J. F. Martin, "Retardation-induced plasmon resonances in coupled nanoparticles," Opt. Lett. **26**, 1096–1098 (2001).
29. E. T. Arakawa, M. W. Williams, R. N. Hamm, and R. H. Ritchie, "Effect of damping on surface plasmon dispersion," Phys. Rev. Lett. **31**, 1127–1129 (1973).
30. R. Younkin, K. K. Berggren, K. S. Johnson, M. Prentiss, D. C. Ralph, and G. M. Whitesides, "Nanostructure fabrication in silicon using cesium to pattern a self-assembled monolayer," Appl. Phys. Lett. **71**, 1261–1263 (1997).
31. J. A. Rogers and R. G. Nuzzo, "Recent progress in soft lithography," Mater. Today **8**, 50–56 (2005).